J. Membrane Biol. 34, 383–408 (1977)

Transport Number Effects in the Transverse Tubular System and Their Implications for Low Frequency Impedance Measurement of Capacitance of Skeletal Muscle Fibers

Peter H. Barry

School of Physiology and Pharmacology, University of New South Wales, Kensington, N.S.W. 2033, Australia

Received 9 November 1976

Summary. It has been shown in an earlier paper that the slow transient decrease in conductance, sometimes referred to as "creep", obtained with small-to-medium hyperpolarizing current or voltage pulses is due to K^+ transport number differences across the walls of the transverse tubular system. Using the same basic numerical analysis and the parameters already obtained experimentally in the previous paper for frog skeletal muscle in a sulphate Ringer's solution, this paper predicts the equivalent membrane capacitance and dynamic resistance due to transport number effects for very low amplitude and low frequency sinusoidal currents from the phase lag of the voltage response behind the current. Such sinusoidal currents *per se* give rise to an equivalent capacitance which increased from less than $1\,\mu F \cdot cm^{-2}$ at 10 Hz to about $16\,\mu F \cdot cm^{-2}$ at 0.01 Hz and to an equivalent dynamic membrane resistance which increases from its instantaneous slope resistance value of $11.7\,k\Omega cm^2$ at 10 Hz to about $16\,k\Omega cm^2$ at 0.01 Hz. Similar small sinusoidal components of current superimposed on depolarizing and hyperpolarizing pulses (25–45 mV) give rise to even greater "capacitances" at low frequencies (e.g., 24–28 $\mu F \cdot cm^{-2}$ at 0.01 Hz). The response due to large sinusoidal currents was also investigated. These transport number effects help to explain the small discrepancies obtained by some workers between experimental and predicted values of skeletal muscle fiber impedances measured in the 1–10 Hz range and would seem to be critical for the interpretation of any skeletal muscle fiber impedance studies done at frequencies less than 1 Hz.

Impedance analysis can provide considerable information regarding the electrical characteristics of a particular system. Indeed for biological cells it can even sometimes give important information concerning the structure and characteristics of the cell membrane itself (e.g., Coster & Smith, 1974*a*, *b*). Thus it is important to distinguish how much of the impedance characteristics are due to the cell membrane itself and how much are due to the geometry of the membrane and physico-chemical effects in the solutions adjacent to it.

It has been known for a long time (Schaefer, Scholmerich & Haass, 1939; Katz, 1949) that when hyperpolarizing currents are applied between

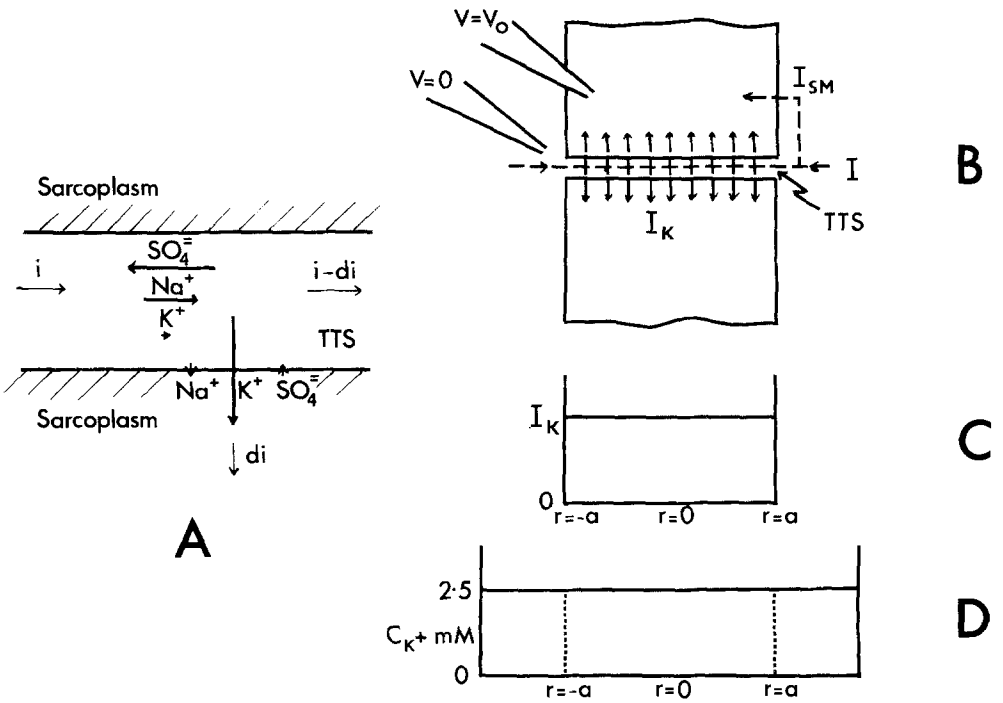

Fig. 1. (*A*) A diagram illustrating current flow between the transverse tubular system (TTS) and the sarcoplasm of a muscle fiber and the effect of transport number differences. At a particular point current i flows radially down the tubules. Over a small incremental distance part of the current, di, crosses the tubular membrane leaving the remainder, $i-di$, to flow radially beyond that increment. The relative fractions of current carried by each ion (given by their transport numbers) is indicated by the length of the appropriate arrows and is shown for a hyperpolarizing current. In particular, it should be noticed that very little of the current in the tubular lumen is carried by K^+, whereas across the tubular wall most of the current is carried by K^+. This will cause a loss of K^+ from the tubular lumen, electroneutrality being automatically conserved by appropriate changes that also take place in $SO_4^=$ and Na^+ concentrations. (*B*) A schematic diagram of a longitudinal cross-section of a muscle fiber showing the current distribution between the surface membrane, I_{SM}, and the walls of the equivalent TTS disc, I_K, at the onset of a hyperpolarizing current pulse. The length of the arrows are intended to be somewhat proportional to the magnitude of the current density. The potential of the sarcoplasm ($V=V_0$) is measured with respect to the external solution ($V=0$). (*C*) A diagram showing the current density crossing the walls of the equivalent TTS disc as a function of radial distance r from the center of the fiber ($r=0$) to its circumference ($r=a$) at the onset of a hyperpolarizing current pulse. (*D*) A diagram showing the initial K^+ concentration profile through the lumen of the TTS and beyond into the external solution (where $r<-a$, $r>a$)

the inside and outside of a muscle fiber there are slow time-dependent changes in the recorded voltage corresponding to a decrease in the measured conductance of that fiber. It was originally suggested (Adrian & Freygang, 1962) that this could be due to transport number effects in the

transverse tubular system of the muscle fiber, resulting in a depletion of K^+ within the tubules, but objections to this hypothesis were later raised (Adrian, Chandler & Hodgkin, 1970*b*). Obviously, even though it is open to the external solution (Huxley, 1964; Page, 1964; Endo, 1966), the transverse tubular system must behave as a very effective unstirred region. It is therefore to be expected (e.g., Dewhurst, 1960; Barry & Hope, 1969*a*; Wedner & Diamond, 1969) that if there are differences in transport numbers between a membrane and adjacent solutions that there should be depletion or enhancement of salt in the unstirred layers or regions adjacent to the membrane, the local concentration changes being mainly balanced by diffusion. This has been experimentally verified in planar wall segments and cylindrical membranes of giant algal cells (Barry & Hope, 1969*a*, *b*). It would therefore also be expected that, since there are differences in ionic transport numbers between the tubular membrane and the lumen of the transverse tubular system (TTS) as indicated in Fig. 1*A* (*see also* Fig. 1*B*, *C* and *D*), there should be local changes in K^+ concentration there. In addition Almers (1972*a*, *b*) carried out a detailed and very elegant experimental investigation of these slow conductance changes and successfully met the objections against the hypothesis of K^+ depletion within the TTS of skeletal muscle fibers.

This decrease in the tubular K^+ concentration (Fig. 2*C*) must result in a concentration gradient in the opposite direction to the applied voltage and hence a transient reduction in the K^+ current at a particular point (*see* Fig. 2*A* and *B*). In the case of both constant voltage and constant current pulses, there should be a predicted drop in the overall current going through the TTS, the current density being minimal at the center of the fibers. As indicated qualitatively in Fig. 2*B* and *C* this drop in the tubular current should be approximately compensated for by an increase in the current crossing the surface membrane of the fiber. For both constant voltage and constant current pulses these effects correspond to a significant transient decrease [e.g., 50%; for further details *see* Barry & Adrian, 1973 (hitherto referred to as *Paper 1*); *see also* Fig. 3] in the effective total conductance of the fiber (time constant 300–600 msec).

Fig. 3*A* and *B* shows the agreement between the theoretically predicted and the experimental curves for both constant voltage and constant current pulses (modification of Figs. 7 and 8 in *Paper 1*). The divergence between the predicted and observed voltage traces at the turn-off of the constant current pulse is discussed in *Paper 1*. It should be emphasized that there was no arbitrary fitting of parameters. The tubular parameters were those obtained or suggested elsewhere in the literature, though in

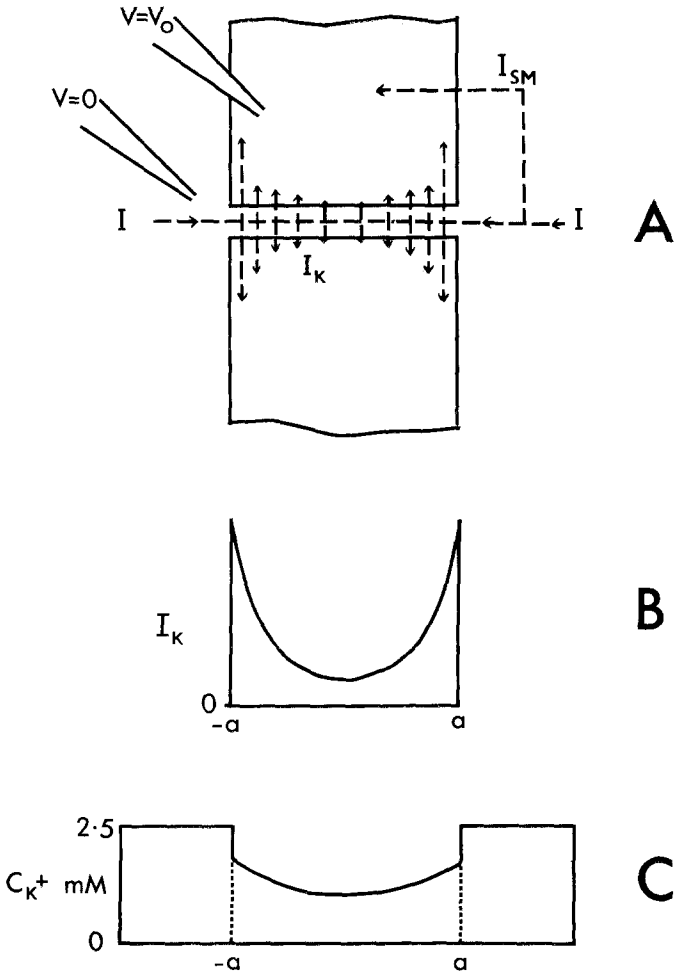

Fig. 2. (*A*) A schematic diagram of a longitudinal cross-section of a muscle fiber showing the computed current distribution between the surface membrane, I_{SM}, and the walls of the equivalent TTS disc, I_K, towards the end of a 2 sec rectangular hyperpolarizing current pulse. The length of the arrows are again intended to be somewhat proportional to the magnitude of the current density. This figure should be compared with Fig. 1*B*. It can be seen that because of K^+ depletion (*see* Fig. 2*C*) maximal at the center of the fiber, where diffusion is least effective, the driving force on K^+ is reduced towards the center of the fiber. Hence the current density is redistributed from the center to the circumference of the fiber and also across the surface membrane. This means that more current is crossing a smaller area of the fiber corresponding to an increase in overall membrane resistance. (*B*) A diagram showing the approximate magnitude of the computed current density crossing the walls of the equivalent TTS disc as a function of radial distance r from the center of the fiber to its circumference ($r=a$) towards the end of a 2 sec pulse. This figure should be compared to Fig. 1*C*. (*C*) A diagram showing the approximate computed K^+ concentration profile through the lumen of the TTS and beyond into the external solution (where $r<-a$, $r>a$). The sudden drop in concentration at $-a$ and a arises because of the small access resistance into the TTS considered in the analysis. This figure should be compared with Fig. 1*D*

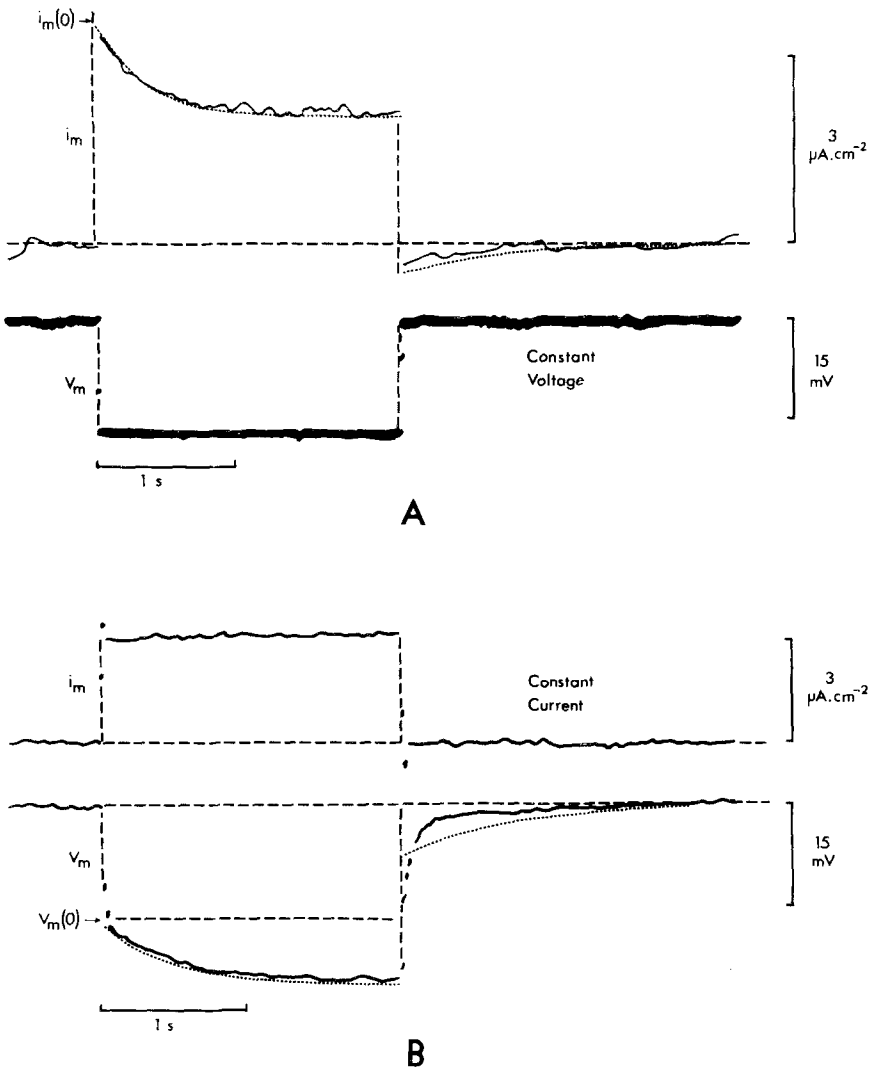

Fig. 3. (*A*) and (*B*) are a modified composite of Figs. 7 and 8 of *Paper 1* and are presented here for convenience to show a comparison of enlargements of experimental records of membrane current and membrane voltage for the same frog sartorius muscle fiber together with the theoretical curve (dotted line) computed from a numerical analysis of transport number effects. In each case they are the average of 8 pulses and the membrane current, i_m, and membrane voltage, V_m, were recorded as $V_2 - V_1$ and V_2 in a 3-electrode set up. For clarity (except for the voltage trace of (*A*)) only the center of the experimental traces has been drawn in. For some further details *see below*. However, for full details see *Paper 1*. (*A*) Experimental membrane current, i_m, (full curve) resulting from a 2 sec rectangular hyperpolarizing voltage pulse (V_m) and the theoretically predicted membrane current (dotted line). $i_m(0)$ is the extrapolated value of the theoretical membrane current at the beginning of the pulse (neglecting the capacity transient). (*B*) Experimental membrane voltage, V_m, (full curve) resulting from a 2 sec rectangular hyperpolarizing current pulse (i_m) and the theoretically predicted membrane voltage (dotted line). $V_m(0)$ is the extrapolated value of the theoretical membrane voltage at the beginning of the pulse (neglecting the capacity transient)

some cases the precise magnitude of the values was open to some debate (*see Paper 1*) and the electrical parameters were those measured experimentally for that particular fiber. In fact, since *Paper 1* had been published, more recent measurements by Mobley and Eisenberg (1975) have confirmed the value of one of the most critical tubular parameters[1] – the fraction of fiber volume occupied by transverse tubules. They found this to be 0.0032, as compared with the figure of 0.003 (Peachey, 1965) used in *Paper 1* and in this present paper. One further point worth commenting on concerns the localization of anomalous rectification (i.e., inward rectification of K^+ ions, e.g., Adrian & Freygang, 1962). Since earlier evidence had indicated that there is anomalous rectification in both the surface and tubular membranes of skeletal muscle fibers (Eisenberg & Gage, 1969), an in *Paper 1*, the rectification parameters were considered to be the same for both the surface and tubular membranes. In additional defence of such on assumption is (1) the good fit obtained in *Paper 1*, particularly for the on-phase of rectangular hyperpolarizing pulses hence validating quantitative impedance predictions for hyperpolarizing pulses, and (2) the fact that rectification is only a secondary effect, certainly as far as qualitative predictions are concerned (e.g., compare the two curves in Figs. 9 and 10).

Now it has already been shown (Segal, 1967; J. Smith, *manuscript in preparation*) under different circumstances that unstirred-layer transport number effects in membranes give rise to very large apparent capacitance effects at very low frequencies (< 1 Hz). In addition Valdiosera, Clausen and Eisenberg (1974*b*) have shown that there is a discrepancy between the impedance measured at very low frequencies (1–10 Hz) and that predicted from the equivalent electrical circuits of the muscle fibers alone, the discrepancy being equivalent to a greater negative phase lag (a greater equivalent capacitance) than that expected from the electrical circuit analysis alone.

It therefore seemed particularly useful to take the data of *Paper 1* for frog muscle fibers where the predictions under rectangular hyperpolarizing current and voltage pulses had been so well fitted by the transport number model and use the numerical analysis appropriately modified to predict the voltage response for a low frequency sinusoidal current input. An impedance analysis was then undertaken in the low frequency range from 0.01–10.0 Hz and it was found that below 1 Hz there was a very significant

1 A 50% divergence in the volume-to-surface ratio of the tubules between the two sets of data was not relevant to this present analysis since $\bar{G}_W$ had been directly determined from R_m (*see* Table 1; determined in *Paper 1* using Eqs. (7), (10) and (11) of that paper).

increase in the negative phase lag, that corresponded to a large equivalent capacitance. A preliminary report of some of the conclusions of this analysis has been published previously (Barry, 1976).

Methods and Details of Numerical Analysis

The experimental membrane parameters used were those that had been obtained by the three-electrode technique on sartorius muscle fibers of *Rana temporaria* and which were given in *Paper 1*. They corresponded to the average parameters for a number of fibers (*see* Tables 2 and 3 of *Paper 1*) and were referred to as model fiber parameters in that paper. These average model fiber parameters, together with the tubular parameters that had been used in that paper, are outlined in Table 1 and corresponded to measurements carried out at a temperature of 20 ± 0.5 °C in a sulphate solution with the following ionic composition in mmole per liter: K^+, 2.5; Na^+, 190; Ca^{2+}, 9; HPO_4^{2-}, 1.08; $H_2PO_4^-$, 0.43; SO_4^{2-}, 104; with the addition of TTX at a concentration of 3.2×10^{-6} molar (10^{-6} g · ml^{-1}) to block action potentials.

The numerical techniques were essentially the same as those outlined in *Paper 1* for constant current pulses. In other words they involved dividing the fiber up into 20 concentric rings of equal radial thickness and the use of numerical difference equations similar to those given in the mathematical analysis of that paper and derived in a later paper (Barry, *in preparation*). The models did not include any real capacitative effects, since, apart from the additional considerable complications that they would add to the analysis, their effects would be small below 2 Hz and negligible below 1 Hz, relative to the transport number effects. In addition this would help to differentiate the effects outlined in this paper from real capacitative effects. At higher frequencies this could introduce some error since the real capacitative current would not have a significant transport number effect, particularly as far as K^+ ions are concerned. In fact for a real capacitance of about 6 μF · cm^{-2} (Adrian, Chandler & Hodgkin, 1969) and a membrane resistance of about 6.6 kΩ · cm^2, using $(1+(\omega\tau)^2)^{-\frac{1}{2}}$ as a measure of the fraction of ionic current going through the membrane resistance, at 0.5 Hz more than 99% of the membrane current would be ionic, at 1 Hz the ionic fraction would be about 97%, at 3 Hz it would still be 80%, although at 10 Hz it will have dropped to about 37%. This means that at 1 Hz transport number effects are overestimated by about 3% and at 3 Hz by about 20%. Since the transport number effects only really become significant at less than 1 Hz and are very small at 3 Hz, the exclusion of real capacitative effects in the analysis is not, therefore, a serious limitation.

The Fortran IV language (McCracken, 1965) was used, and the time after the onset of the pulse was incremented in steps, Δt. However, now at the beginning of each time step, after time t, the total current I, was calculated from the expression

$$I = I_R + \Delta I_p \sin \omega t \tag{1}$$

where ΔI_p is the peak value of the sinusoidal component of current used (either 0.01 or 2.25 μA · cm^{-2}) I_R is the constant rectangular component of current, that generally started long (~10–12 sec) before the sinusoidal component started, and ω was the radial frequency in radian per sec ($=2\pi f$, where f is in Hz). The membrane current was then computed, and using a fourth-order Runge-Kutta routine (Ralston, 1965) the change in concentration and hence the new concentration in each of the 20 rings was computed at the later time $t+\Delta t$. The actual Runge-Kutta equations used were Eqs. (72)–(74) of *Paper 1*. There was, however, a significant modification to the current-finding subroutine. In *Paper 1* it had been found that if a reasonably good trial solution of the tubular current was used and then a fraction

(1/7) of the excess current remaining at the central ring was subtracted from it that there was a rapid convergence of the trial current to its correct value. Whilst this converged well for the conditions in *Paper 1*, it was found that for other conditions or data, and in particular for a sine-wave current input, that it no longer converged. In addition the iterative procedure used for correcting changes in conductance with voltage would not readily converge when the voltage differed significantly from the value at which the conductance was experimentally measured. The first problem, which only arose with clamped (constant or sinusoidal) current pulses, was overcome by using a Newton-Raphson procedure (e.g., Ralston, 1965, p. 332) whereby the new correction to the trial current δI_{n+1} is related to the old correction δI_n by

$$\delta I_{n+1} = \frac{f(I_{n+1}) \cdot \delta I_n}{f(I_n) - f(I_{n+1})}. \tag{2}$$

Where $f(I_n)$ is the excess current at the central ring for trial current, I_n, and $f(I_{n+1})$ is the excess current for trial current $I_{n+1} (= I_n + \delta I_n)$. Hence the new value of the trial current becomes:

$$I_{n+2} = I_{n+1} + \delta I_{n+1}. \tag{3}$$

In addition to converging under all conditions tested this also proved to be in all cases much faster at converging than the fractional method used in *Paper 1*.[2] In contrast to *Paper* 1 the maximum error of this current $\delta I_n / I_n$ had to be decreased to $< 10^{-10}$ for both the small 0.01 μA sinusoidal current computations and the larger 2.25 μA sinusoidal current computations.[3]

The second problem, for correcting for changes in conductance with voltage due to anomalous rectification, was overcome by using Newton's method of solution of equations (e.g., Sokolnikoff & Redheffer, 1958, pp. 684–5).

Having chosen a trial value of I_o for the tubular current, the value of the membrane potential, V_o, was estimated from the corrected surface membrane resistance using the same equation as used before for the analysis in *Paper I*, i.e.,

$$V_o = \frac{(I - I_o) \times R_{sm}}{G(V_o)} \tag{4}$$

where I is the total current, R_{sm} is the resistance of the surface membrane at a p.d. of -15.0 mV and G the factor used to compensate for changes in conductance with voltage is given by

$$G(V_o) = g_1 + g_2 V_o + g_3 V_o^2 + g_4 V_o^3. \tag{5}$$

Instead of the very simple iterative procedure previously used, Newton's method was used as follows to solve:

$$F(V_o) = \frac{(I - I_o) R_{sm}}{G(V_o)} - V_o = 0 \tag{6}$$

$$V_{n+1} = V_n - \frac{F(V_o)}{F'(V_n)} \tag{7}$$

---

2 In contrast, for clamped voltage pulses the fractional method was always reliable and proved to be slightly faster than the Newton-Raphson technique (in this case the fraction represented all of the excess current).

3 In a few instances during the larger sinusoidal computations, the error had to be temporally increased to $< 10^{-7}$–10^{-9} during that part of the cycle in which the total membrane current approached zero.

where V_n represents the n^{th} trial solution for V_o and $F'(V_n)$ represents the derivative of $F(V_n)$, the solution being considered to have been reached when

$$F(V_n)/V_n < 10^{-10} \quad \text{for } \Delta I_p = 0.01\ \mu\text{A} \cdot \text{cm}^{-2}$$

and for $\Delta I_p = 2.25\ \mu\text{A} \cdot \text{cm}^{-2}$.

As before (*see Paper 1*) there should be a maximum bound on the time step for the given number of rings (20) for stability of the procedure. However, in contrast to *Paper 1*, there was some limited varying of the time step throughout a particular computation to increase efficiency and still maintain accuracy. For the first 2 sec of the constant rectangular current pre-pulses (time constant ~600–700 msec) $\Delta t = 0.001$, whereas for the remainder of the rectangular pre-pulse $\Delta t = 0.005$. During most of the sinusoidal parts of the pulse, longer time steps (e.g., $\Delta t = 0.005$ for frequencies between 0.01–1.0 Hz, and $\Delta t = 0.001$ and 0.0005 for frequencies of 5 and 10 Hz, respectively) were used. On the other hand, in order to accurately measure the time lag of the voltage behind the current, the time step was decreased by a factor of 5, 10 or 50 times for those parts of the cycle between the critical peak and zero points of the sinusoidal component of the current and the corresponding peak and zero points of the sinusoidal component of the voltage.

Using a CDC 6600 computer (with its 15 decimal digit single precision) the modified program was rather faster than before and, whether calculating a rectangular or sinusoidal current pulse, at a fixed time step $\Delta t = 0.001$, took about 200 sec of computing time for a pulse of 4 sec duration. For the very low frequency curves computing times could still be very considerable. However, now using the variable time step method outlined above, a typical 200 sec 2 cycle 0.01 Hz pulse decreased in time of computation from about 9000 sec to under 2000 sec. A comparison of runs at 0.01 Hz and 0.1 Hz by the variable and fixed time step methods (the latter being at the smallest time step throughout to check the accuracy of the variable time step method) gave agreement between time lags to within 1 part in 290 and 1 part in 245, respectively, and agreement between peak voltages to better than 2 parts in 10^4.

Results

As already indicated the calculations were based on the model muscle fiber parameters outlined in Table 1. Three sets of computations were done. In each case the dependence of conductance on voltage, due to anomalous rectification, was taken into account. This relationship between the conductance factor (G) and the voltage (i.e., the change in membrane potential due to the applied current) (V) was taken to be as follows (*see* Table 1)

$$G = g_1 + g_2 V^* + g_3 V^{*2} + g_4 V^{*3} \tag{8}$$

where

$$V^* = V - \frac{RT}{F} \ln [K]/[K]_o \tag{9}$$

where $[K]_o$ is the initial concentration of potassium in the transverse tubular system and is also the bulk solution concentration and where $[K]$

Table 1. Typical frog muscle model fiber parameters used for computing impedance data (see Paper I for further details)

Conductance of tubular lumen, $G_L = 10^{-2}\ \Omega^{-1} \cdot \text{cm}^{-1}$
The fraction of fiber volume occupied by tubules[a], $\rho = 0.0030$ (with an additional 0.001 for the volume of the longitudinal tubules).
TTS network factor[a], $\sigma = 0.5$.
Fiber radius, $a = 51\ \mu\text{m}$.
Electrical access resistance of the TTS, $r_s = 100\ \Omega\text{cm}^2$.
Concentration of K^+ in the TTS, $C_K = 2.5\ \text{mM} \times \text{liter}^{-1}$.
Effective radial conductance of the lumen of the TTS per unit volume of fiber, $\bar{G}_L = 1.5 \times 10^{-5}\ \Omega^{-1} \cdot \text{cm}^{-1}$.
Tubular fraction of conductance, $f_T = 0.66$.
Diffusion coefficient of K^+ in the tubular lumen, $D_K = 1.6 \times 10^{-5}\ \text{cm}^2 \cdot \text{sec}^{-1}$.

Conductance parameters that vary with the driving force across the membrane to account for anomalous rectification (*see* Fig. 5 of *Paper 1* based on data of Adrian & Freygang, 1962).

$g_1 = 0.559642 \quad g_2 = -25.5904 \quad g_3 = 322.869 \quad g_4 = 4783.23$

Where the conductance factor

$$G(V) = g_1 + g_2 \cdot V^* + g_3 \cdot V^{*2} + g_4 \cdot V^{*3}$$

with V^* in volts and

$$V^* = V - \frac{RT}{F} \ln [\text{K}]/[\text{K}]_o$$

where V is the change in membrane p.d. across the tubular walls; R, T, F are the gas constant, Temperature in °K and the Faraday; $[\text{K}]_o$ and $[\text{K}]$ are the initial and later K^+ concentrations within the TTS.
$R_{sm} = 10.41\ \text{k}\Omega\text{cm}^2$ (at -15.0 mV hyperpolarizing), $= 34.68\ \text{k}\Omega\text{cm}^2$ (at 0.0 mV).
$\bar{G}_W = 0.040\ \Omega^{-1} \cdot \text{cm}^{-3}$ (at -15.0 mV hyperpolarizing), $= 0.0224\ \Omega^{-1}\ \text{cm}^{-3}$ (at 0.0 mV).

Chord (R_m) *and slope resistances* (dV/dI) *at onset and termination of long* (10–12 sec) *constant current pulses of magnitude* $2.25\ \mu\text{A} \cdot \text{cm}^{-2}$.

R_m at onset of hyperpolarizing pulse ($V = -14.95$ mV)	$= 6.64\ \text{k}\Omega\text{cm}^2$
R_m at end of hyperpolarizing pulse ($V = -21.88$ mV)	$= 9.72\ \text{k}\Omega\text{cm}^2$
dV/dI at end of hyperpolarizing pulse	$= 4.67\ \text{k}\Omega\text{cm}^2$
R_m at onset of depolarizing pulse ($V = +40.42$ mV)	$= 17.96\ \text{k}\Omega\text{cm}^2$
R_m at end of depolarizing pulse ($V = +45.64$ mV)	$= 20.29\ \text{k}\Omega\text{cm}^2$
dV/dI at end of depolarizing pulse	$= 5.19\ \text{k}\Omega\text{cm}^2$
Slope resistance (dV/dI) at the origin ($V = 0.0$)	$= 11.72\ \text{k}\Omega\text{cm}^2$

[a] In practice the effects of the longitudinal tubule volume was taken into account (*see Paper I*) by increasing ρ to 0.0040 and decreasing σ to 0.375 so that $\sigma\rho$ was still 1.5×10^{-3}.

is the tubular concentration at any later time (t). For a calculation of the conductance of the surface membrane, V^* is taken to be equal to V.

In the first two sets of computations only a small sinusoidal component of current (peak amplitude $0.01\ \mu\text{A} \cdot \text{cm}^{-2}$) was used. The small amplitude

meant that the membrane conductance remained effectively constant and that there was minimal distortion of the sinusoidal nature of the voltage waveform. In fact the voltage was equally shifted in phase at each point throughout the cycle (*cf.* the maximum differences in time lags given in Tables 2 and 3), and thus it is quite valid to calculate an equivalent capacitance and dynamic resistance from these time lags.

In the second set (*B*) long 2.25 $\mu A \cdot cm^{-2}$ rectangular hyperpolarizing and depolarizing currents were used with the small sinusoidal component superimposed after the initial transient response to the rectangular component had settled down (the time constant for the transport number effects was 0.8 sec, and 10–12 sec of this pre-pulse was allowed before the sinusoidal component was started; cp. Fig. 7) in order to compute the equivalent capacitance during such hyperpolarizing and depolarizing pulses.

In the third set of computations (*C*) a very large sinusoidal current (amplitude 2.25 $\mu A \cdot cm^{-2}$) with no dc component was used. There was, however, now considerable distortion of the voltage waveform from a sine wave, as a result of anomalous rectification.

In each case the range of frequencies investigated was from 0.01 to 10.0 Hz. The current input always started from zero with the hyperpolarizing half-cycle and the analysis was continued until a steady-state had been reached. This was taken to be the cycle (indicated by an *f* in Tables 2–4) after which there was no change in the time lag within the accuracy of measurement and in which the maximum voltage amplitude differed by less than 0.1 % (or 0.01 % in Table 4) from its value in the cycle following.

A. Computed Impedance Data for a Small 0.01 $\mu A \cdot cm^{-2}$ *Sinusoidal Current Input for the Model Muscle Fiber*

Table 2 summarizes the basic results. The time lag of the voltage curve behind the current curve is measured at the peak values of the voltage in both the hyperpolarizing and depolarizing directions, and at the zero points following them. Similarly the voltage amplitude was measured at both the peak of the hyperpolarizing and depolarizing cycles.

The phase angle ϕ was calculated from the average time lag, Δt (given in Table 2) by using the relationship

$$\phi = \omega \Delta t = 2\pi f \Delta t \text{ (radians)} = 360 f \Delta t^0 \qquad (10)$$

Table 2. Computed impedance data for a typical frog muscle model fiber with a very small sinusoidal current input (amplitude 0.01 $\mu A \cdot cm^{-2}$)

Frequency of current (Hz)	Cycle No.[a]	Time lag (sec)		Peak voltage (mV)	
		Avr.[b]	Max. diff.[c]	Avr.[d]	Max. diff.[e]
0.01	1*f*	0.255	0.001	0.159	0.001
0.05	2*f*	0.239	0.001	0.156	0.001
0.1	2*f*	0.198	0.001	0.149	0.001
0.2	2*f*	0.119	0.001	0.135	0.001
0.4	4*f*	0.046	0.001	0.124	0.001
0.5	4*f*	0.032	0.001	0.122	0.001
1.0	7*f*	0.009	0.000	0.119	0.001
5.0	14*f*	0.0004	0.0001	0.117	0.001
10.0	20*f*	0.0001	0.0000	0.117	0.001

[a] The *f* after the cycle number indicates that a steady-state had been reached (i.e., no change in the time lags within the accuracy specified and the maximum voltage amplitude within 0.1% of its value in the next few cycles following).

[b] This column presents the average of the four time lag computations within the cycle – the lag of the hyperpolarizing and depolarizing peak voltages and the two zero voltages behind the equivalent points in the current cycle.

[c] This column represents the maximum difference from the average of the time lags (rather than the SEM) of the voltage behind the sinusoidal current input in order to emphasize the lack of distortion of the voltage trace.

[d] This column represents the average between the peak voltages in the hyperpolarizing and depolarizing phases of the cycle, respectively.

[e] This column represents the maximum difference between the average peak value and the peak hyperpolarizing and depolarizing parts of the cycle.

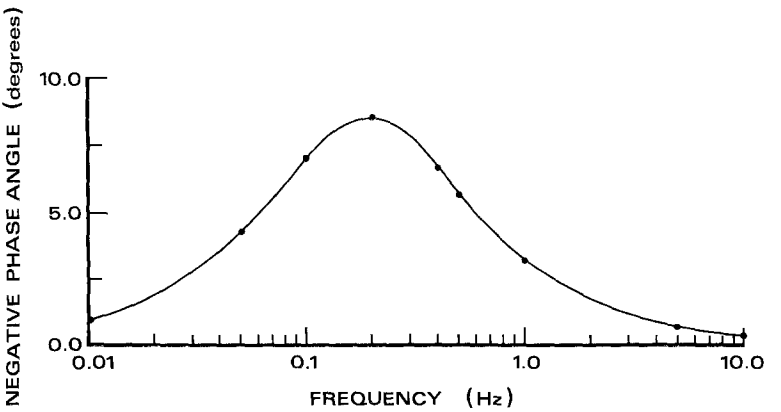

Fig. 4. The predicted phase angle between sinusoidal current and voltage, at different frequencies, due solely to transport number effects. This negative phase angle, representing the lag of the voltage behind the current, was computed from data for a frog muscle model fiber using the numerical analysis discussed in the text for a peak current of 0.01 $\mu A \cdot cm^{-2}$. Note the logarithmic frequency scale in this figure and in Figs. 5–6 and 8–11

and the phase angle is shown plotted as a function of frequency in Fig. 4. There is no significant change in the time lag (Table 2) and hence in the phase lag throughout the cycle. The curve is a fairly symmetrical bell-shaped curve with a maximum phase angle of about $-8.5°$ occurring at about 0.2 Hz. The phase angle drops to just less than $-1°$ above 5 Hz and below 0.01 Hz.

Following the *RC* electrical circuit analogue (a sinusoidal current into a resistance and capacitance in parallel) the equivalent dynamic membrane resistance R_m, was calculated from the impedance, Z_m (average peak voltage/0.01 μA, obtained from Table 2) and the phase angle, ϕ, obtained from Table 2 by using Eq. (10) and the relationships

$$R_m = Z_m \cdot (1 + (\omega \tau)^2)^{\frac{1}{2}} \tag{11}$$

where

$$\tan \phi = \omega \tau \tag{12}$$

and τ, the time constant, may be defined by

$$\tau = R_m C_m. \tag{13}$$

Fig. 5 illustrates how in spite of this correction the dynamic membrane resistance is still dependent on frequency, being constant and approximately equal to the actual membrane slope resistance R_m^*, of 11.7 kΩ · cm^2 (with no transport number effects present; *see* Table 1) for frequencies higher than about 5.0 Hz, and increasing in magnitude as the frequency decreased, reaching a maximum value of about 16 kΩ · cm^2 at 0.01 Hz.

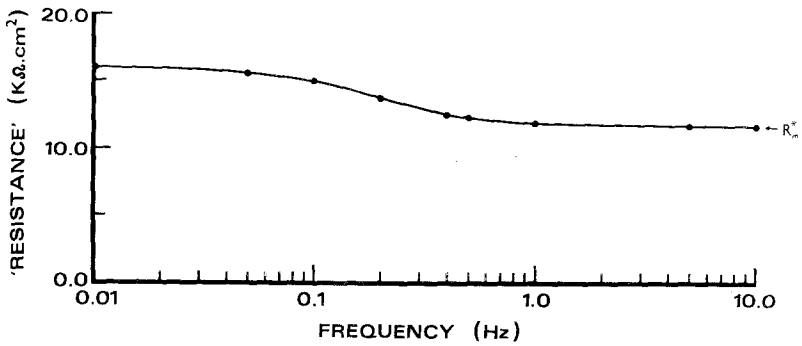

Fig. 5. The predicted equivalent dynamic membrane resistance, for sinusoidal currents of different frequencies, due to transport number effects. These points were calculated from the phase angle data (Fig. 4) and peak values of membrane current and voltage given in Table 2 as discussed in the text. R_m^* represents the instantaneous membrane slope resistance ($dV/dI = 11.72$ kΩ · cm^2) without transport number effects. The conditions, as in Fig. 4, were for a peak current of 0.01 μA · cm^{-2}

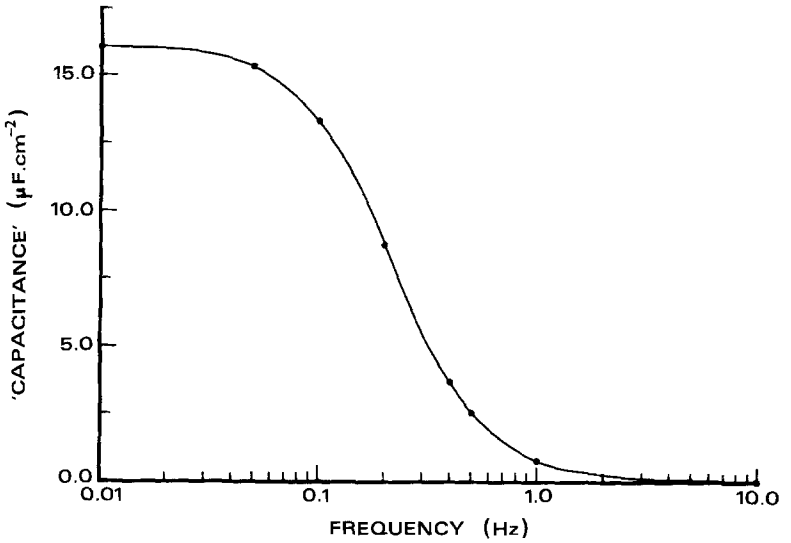

Fig. 6. The predicted equivalent capacitance ('capacitance'), for sinusoidal currents of different frequencies, due solely to transport number effects. These points were calculated from the phase angle data (Fig. 4) and the equivalent dynamic membrane resistance (Fig. 5). The conditions, as in Figs. 4 and 5, were for a peak current of 0.01 $\mu A \cdot cm^{-2}$

From these values of R_m and ϕ the equivalent capacitance, C_m, was calculated using Eqs. (12) and (13), and is shown in Fig. 6 plotted as a function of frequency. It may be seen from the figure that C_m is less than 1 $\mu F \cdot cm^{-2}$ for frequencies greater than 1.0 Hz but that it rises sharply and levels off to a value of almost 16 $\mu F \cdot cm^{-2}$ for frequencies less than about 0.05 Hz.

B. Computed Impedance Data for a 0.01 $\mu A \cdot cm^{-2}$ *Sinusoidal Current Superimposed on* 2.25 $\mu A \cdot cm^{-2}$ *Rectangular Depolarizing and Hyperpolarizing Pulses*

In this set of computations very long rectangular hyperpolarizing (12 sec) and depolarizing (10 sec) current pre-pulses were used, so that the initial transient response to the rectangular pre-pulse had died away before the small sinusoidal component of current was superimposed on it as shown in Fig. 7. The anomalous rectification was illustrated by the fact that changes in potential at the end of the rectangular pre-pulse were -22 and $+46$ mV for the hyperpolarizing and depolarizing pulses, respectively.

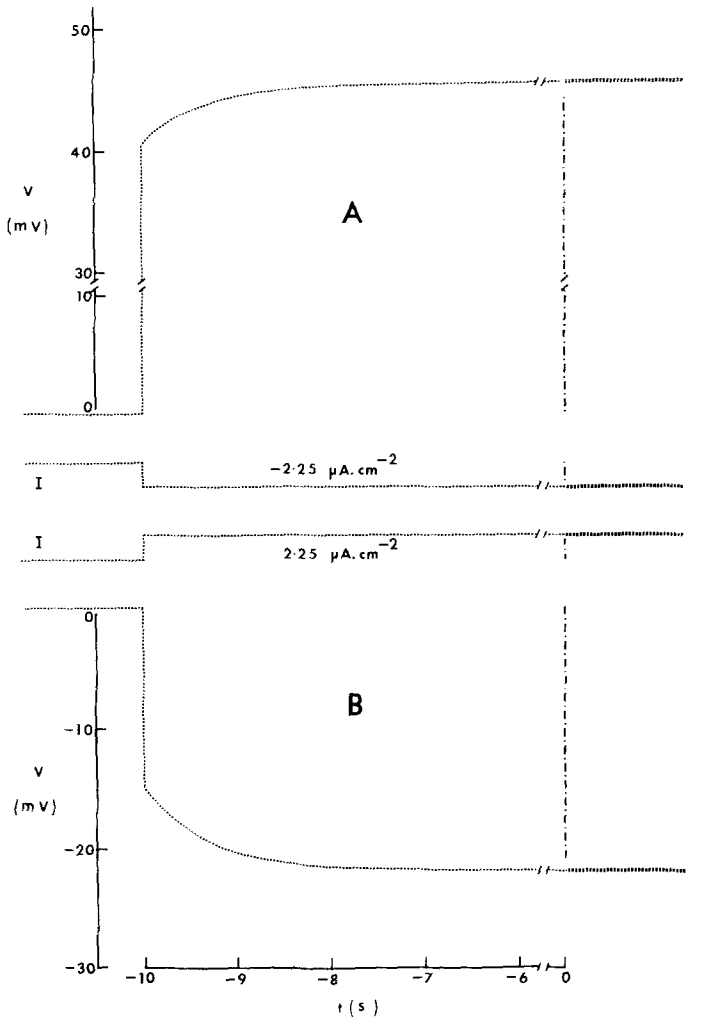

Fig. 7. The transient voltage response, during the long (e.g., 10 sec) 2.25 $\mu A \cdot cm^{-2}$ rectangular hyperpolarizing and depolarizing current pre-pulses due to transport number effects. These curves were computed using the model fiber parameters, the calculations being the ones used to obtain the starting conditions at time $t=0$ for the impedance analysis. The thicker dotted lines represent the small (0.01 $\mu A \cdot cm^{-2}$) superimposed sinusoidal current and resultant voltage traces starting at time $t=0$ at the end of the 10 sec pre-pulse used for the analysis. I represents the membrane current and V the resulting change in voltage across the muscle membrane. (*A*) represents the depolarizing current and voltage response and (*B*) the hyperpolarizing current and voltage response. Note the breaks in the time scale of the pre-pulses which were put in for diagrammatic purposes only. The diagram thus clearly emphasizes that a steady-state has been reached as far as each voltage response is concerned and also shows the anomalous rectification that has been included in the analysis; illustrated by the fact that change in voltage in the depolarizing direction is approximately double that in the hyperpolarizing direction

Table 3. Computed impedance data for a typical frog muscle model fiber with a very small sinusoidal current (amplitude 0.01 $\mu A \cdot cm^{-2}$) superimposed (*A*) on a long rectangular hyperpolarizing pulse (2.25 $\mu A \cdot cm^{-2}$ amplitude) and (*B*) on a long rectangular depolarizing pulse ($-2.25\ \mu A \cdot cm^{-2}$ amplitude)

Frequency of current (Hz)	Cycle No.	Time lag (sec)		Peak voltage change[a] (mV)	
		Avr.	Max. diff.	Avr.	Max. diff.
(*A*) *Hyperpolarizing pulse*					
0.01	1*f*	0.193	0.001	0.0708	0.0001
0.05	1*f*	0.189	0.001	0.0702	0.0001
0.1	2*f*	0.177	0.001	0.0685	0.0000
0.2	2*f*	0.142	0.000	0.0637	0.0000
0.5	4*f*	0.061	0.001	0.0537	0.0001
1.0	4*f*	0.0207	0.0001	0.0491	0.0001
5.0	15*f*	0.0010	0.0001	0.0468	0.0001
10.0	10*f*	0.0003	0.0001	0.0467	0.0001
(*B*) *Depolarizing pulse*					
0.01	1*f*	0.151	0.015	0.0627	0.0001
0.05	2*f*	0.141	0.003	0.0620	0.0001
0.1	2*f*	0.118	0.002	0.0604	0.0001
0.2	2*f*	0.072	0.001	0.0572	0.0001
0.5	4*f*	0.020	0.001	0.0536	0.0001
1.0	5*f*	0.0061	0.0002	0.0526	0.0001
5.0	21*f*	0.0003	0.0001	0.0520	0.0001
10.0	6*f*	0.00005	0.00005	0.0520	0.0002

[a] The layout and terminology used is the same as for Table 2 except that in column 5 the peak voltage *change* is used instead of the peak voltage in the former table.

The phase angles, ϕ, were calculated, as before, in both cases from the time lag data in Table 3 and are shown in Fig. 8 as a function of frequency. In comparison to the situation in the previous section (*A*): for the response during the hyperpolarizing pulse, the maximum phase angle was slightly larger (about $-11.6°$) and occurred at a higher frequency (0.35 Hz); whereas for the depolarizing pulse response, although the maximum phase angle was smaller (about $-5.2°$), it did occur at the same frequency as before (0.2 Hz).

Fig. 9 illustrates the equivalent dynamic membrane resistance, R_m, calculated as before (using Eqs. (10) and (11) from the impedance Z_m, calculated as $\Delta V/0.01\ \mu A$, ΔV being obtained from Table 3). R_m is still very dependent on frequency for both hyperpolarizing and depolarizing pulses. In the hyperpolarizing case R_m is constant and approximately equal to the instantaneous membrane slope resistance $R_m^h(\Delta V/I = 4.7\ k\Omega \cdot cm^2$ at

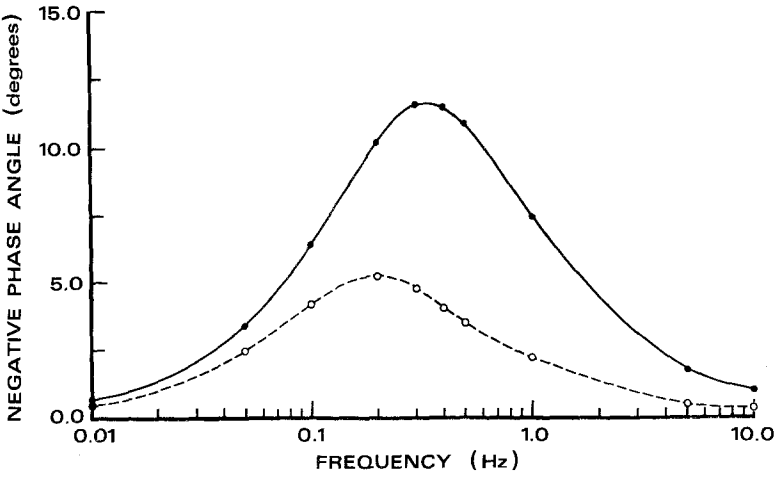

Fig. 8. The predicted phase angle between sinusoidal and voltage, at different frequencies, due solely to transport number effects. This negative phase angle was computed from data for a frog muscle fiber as in Fig. 4, but in this case for a small 0.01 $\mu A \cdot cm^{-2}$ sinusoidal component of current superimposed on rectangular 2.25 $\mu A \cdot cm^{-2}$ hyperpolarizing and depolarizing pulses in the manner illustrated in Fig. 7. The filled circles (with the solid line) represent the response for the hyperpolarizing pulse and the open circles (with dashed line) represent the response for the depolarizing pulse

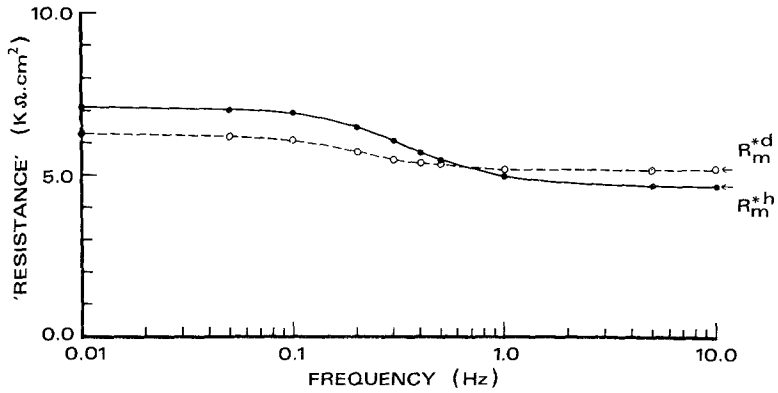

Fig. 9. The predicted equivalent dynamic membrane resistance, for sinusoidal currents of different frequencies, due to transport number effects. As in Fig. 5, the points were calculated from the phase angle data (Fig. 8) and peak values of membrane current and voltage (Table 3) as discussed in the text. R_m^{*h} and R_m^{*d} represent the instantaneous membrane slope resistance (dV/dI) at the end of the constant rectangular hyperpolarizing and depolarizing pre-pulses, respectively. Again the filled circles (with the solid line) and the open circles (with the dashed line) represent the dynamic resistances during the 2.25 $\mu A \cdot cm^{-2}$ rectangular hyperpolarizing and depolarizing pulses, respectively

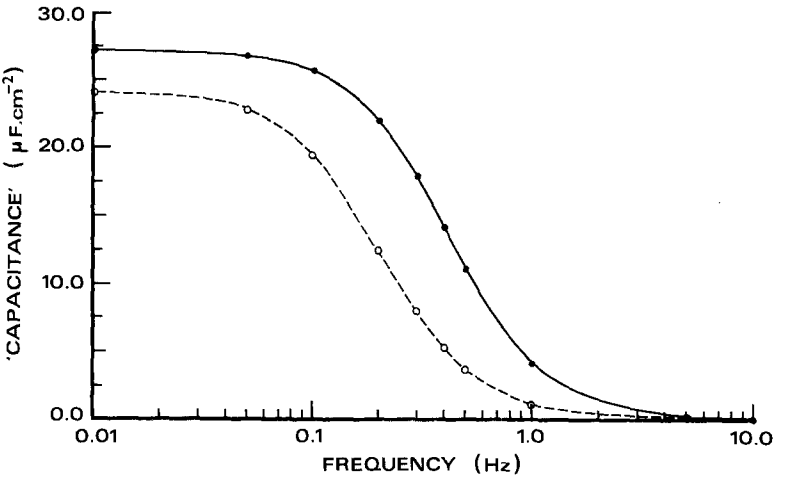

Fig. 10. The predicted equivalent capacitance ('capacitance'), for sinusoidal currents of different frequencies, due solely to transport number effects. As in Fig. 6 the points were calculated from the phase angle data (Fig. 8) and the equivalent dynamic membrane resistance (Fig. 9). Again the filled circles (with the solid line) and the open circles (with the dashed line) represent the equivalent capacitance during the 2.25 $\mu A \cdot cm^{-2}$ rectangular hyperpolarizing and depolarizing pulses, respectively

the end of the rectangular hyperpolarizing current pulse by itself. (*See* Table 1 – no further transport number effects – for frequencies above 1.0 Hz.) It increased in magnitude, however, as the frequency decreased, reaching a maximum of 7 $k\Omega cm^2$ at very low frequencies (i.e., less than 0.1 Hz).

However, although the depolarizing pulse curve followed the shape of the hyperpolarizing one, the relative change in dynamic resistance as the frequency decreased was rather less. At frequencies greater than 1.0 Hz the dynamic resistance was again constant and equal to a slightly higher instantaneous membrane slope resistance $R_m^d(dV/dI = 5.2\ k\Omega cm^2$ at the end of the rectangular depolarizing pulse by itself; Table 1 – with no further transport number effects) whereas at frequencies less than 0.1 Hz it had risen to a steady maximum value of just over 6 $k\Omega cm^2$. In spite of the large difference in dc resistance of the membrane in both cases (e.g., 6.6:9.7, Table 1 and Fig. 7) it should be noted that the instantaneous slope resistance and the dynamic membrane resistances R_m, are remarkably similar for the two pulses.

There is now also an even greater equivalent capacitance than before (cp. Figs. 10 and 6) for both pulses, as is illustrated in Fig. 10. This was calculated as in section *A*, from the data of Table 3 by using Eqs. (11)–(13).

For the hyperpolarizing pulse the equivalent capacitance, C_m, is less than 1 $\mu F \cdot cm^{-2}$ for frequencies greater than 3 Hz. Again C_m rises sharply as in Fig. 6 as the frequency is decreased, but now it rises to a maximum steady value of about 27 $\mu F \cdot cm^{-2}$ below about 0.05 Hz. The depolarizing pulse curve follows the same trend though it is shifted slightly to the left. C_m is less than 1 $\mu F \cdot cm^{-2}$ for frequencies greater than 1.2 Hz and also rises sharply at slightly lower frequencies to a maximum steady value of about 24 $\mu F \cdot cm^{-2}$ below about 0.02 Hz.

C. *Computed Impedance Data for a Large* 2.25 $\mu A \cdot cm^{-2}$ *Sinusoidal Current Input for the Model Muscle Fiber*

The computations are similar to those already discussed in section *A*. However, the large current means that the rectification characteristics are very significant and will give rise to considerable distortion of the voltage waveform from a pure sine wave. This means, as is indicated in Table 4, that (1) the peak voltage for the hyperpolarizing part of the cycle is very much less than that for the depolarizing part, and (2) there is a considerable

Table 4. Computed impedance data for a typical frog muscle model fiber with a sinusoidal current input of very large magnitude (amplitude 2.25 $\mu A \cdot cm^{-2}$)

Frequency of current (Hz)	Cycle No.[a]	Time lag of voltage[b] (sec)				Peak voltage[c] (mV)	
		Δt_m^h	Δt_o^h	Δt_m^d	Δt_o^d	V_m^h	V_m^d
0.01	$1f$	0.194	0.232	0.152	0.288	21.87	45.64
0.05	$2f$	0.210	0.174	0.164	0.277	21.72	45.45
0.1	$2f$	0.244	0.132	0.166	0.220	21.09	44.92
0.2	$2f$	0.211	0.082	0.133	0.131	19.14	43.66
0.5	$4f$	0.0741	0.0263	0.0555	0.0349	16.25	41.61
1.0	$7f$	0.0223	0.0081	0.0188	0.0095	15.35	40.81
5.0	$20f$	0.0010	0.0003	0.0009	0.0003	14.96	40.44
10.0	$25f$	0.00025	0.00009	0.00022	0.00009	14.95	40.42

[a] An f following the cycle number indicates that a steady-state had been reached (i.e., no change in the time lag within the accuracy specified and maximum voltage amplitude within 0.01 % of its value in the cycle following).

[b] Δt_m^h, Δt_m^d refer to the time lag at the peak of the hyperpolarizing and depolarizing voltages, respectively.
Δt_o^h, Δt_o^d refer to the time lag of the zero voltage following the hyperpolarizing and depolarizing parts of the cycle, respectively.

[c] V_m^h and V_m^d refer to the peak values of the voltage in the hyperpolarizing and depolarizing directions, respectively.

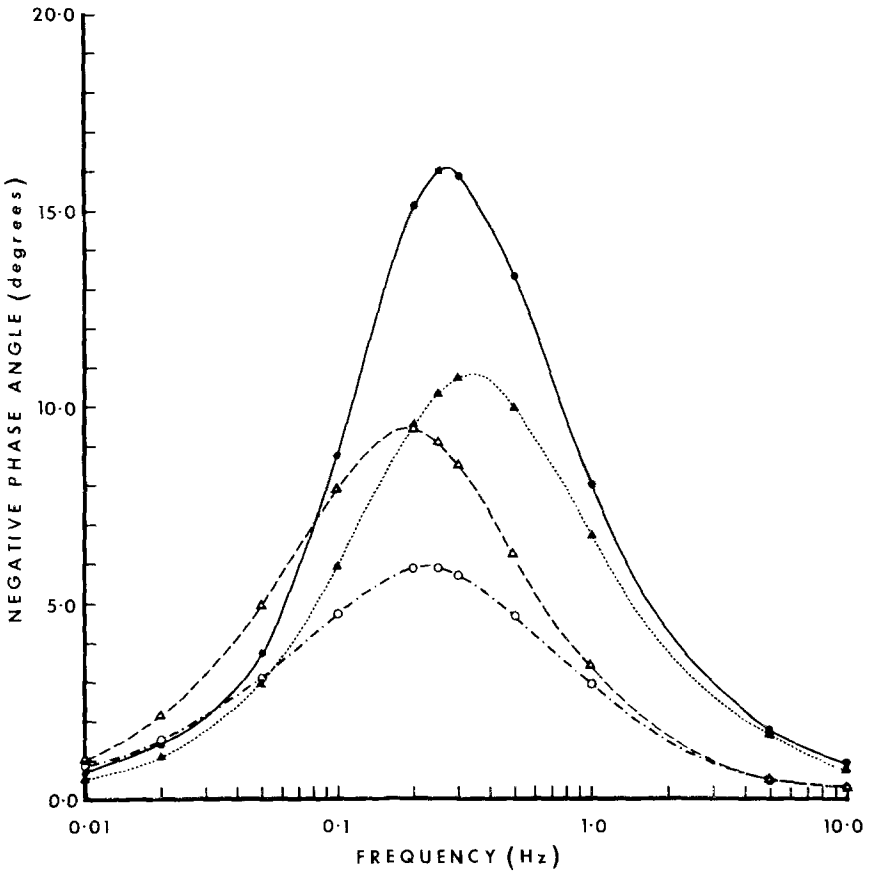

Fig. 11. The predicted phase angle between sinusoidal current and voltage at different frequencies due solely to transport number effects. As in Fig. 4 this was computed from data for a frog muscle model fiber using the numerical analysis discussed in the text. In this case, however, a very large sinusoidal current (peak amplitude $= 2.25\ \mu A \cdot cm^{-2}$) was used by itself. The filled circles (with the solid line) and the filled triangles (with the dotted line) represent the phase lags measured from the peak values of current in the hyperpolarizing and depolarizing parts of the cycle, respectively, whereas the open circles (with dotted-dashed line) and the open triangles (with the dashed line) represent the phase lags measured from the zero values of current at the end of the hyperpolarizing and depolarizing phases of the cycle, respectively. The difference between the 4 curves is due mainly to the anomalous rectification included in the analysis

change in the time lag throughout the cycle. The phase lags for the two peaks were calculated as before from the appropriate time lags and are shown in Fig. 11 as a function of frequency. These phase lags are in fact larger than those obtained previously (*cf.* Figs. 4 and 8). However, all that can really be said is that they are capacitative in nature, since the effect appears to be equivalent to that produced by an anomalous capacitance

that varies somewhat throughout the cycle. From the time lags and impedances computed at the two peaks, one could try to calculate some sort of apparent equivalent capacitance. For example, at 0.1 Hz such a calculation would lead to values of about $26\,\mu F \cdot cm^{-2}$ and $8\,\mu F \cdot cm^{-2}$ for the peak parts of the hyperpolarizing and depolarizing phases of the cycle, respectively. The considerable amount of sine wave distortion, indicated by the difference in these two values and in the sets of time lag values given in Table 4, really makes the validity of such calculations from a straightforward analysis of time lags extremely dubious and thus will not be pursued.

Discussion

This paper first of all considers experimental results (*see Paper 1*) on sartorius muscle fibers in which transport number effects have been shown to cause a slow transient decrease in resistance during rectangular current and voltage clamped pulses. The same basic numerical model and the model fiber parameters that represented the average measurements for a number of fibers in the former paper were used in this paper and it was shown how the model (with some modifications to accept a sinusoidal input) could be used to predict the response of the same model fiber to a sinusoidal current input.

It was then shown that these transport number effects give rise to a very significant phase lag of the voltage response (i.e., negative phase angle) behind the current, especially at frequencies below 1 Hz. Such a phase lag mimics the effect of a very large capacitance and an additional component of resistance and might be mistaken for such if the role of transport numbers were not appreciated. The way in which such frequency-dependent transport number equivalent parameters would combine with the normal capacitance and resistance is shown in Fig. 12 for a modification of the simple lumped equivalent circuit of a muscle fiber. At frequencies greater than 10 Hz, or in the absence of transport number effects, the equivalent transport number capacitance, C_{TN}, and resistance, R_{TN}, would both reduce to zero, and the circuit would reduce to the normal simple lumped equivalent circuit,[4] whereas below 1 Hz they would both become very significant.

4 Of course, in order to accurately describe a normal muscle fiber at frequencies greater than about 10 Hz, a more complicated equivalent circuit—a Hybrid or Disk model (e.g., Valdiosera, Clausen & Eisenberg, 1974*a*, *b*)—should be used which correctly allows for the electrical properties of the transverse tubular system.

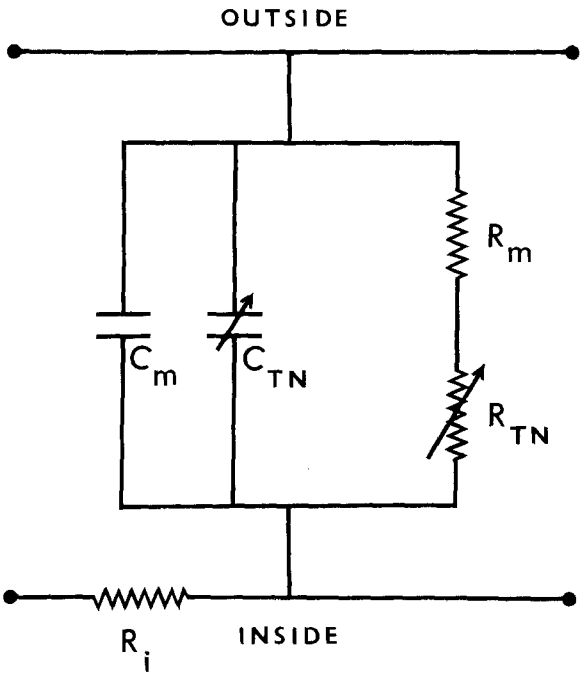

Fig. 12. An equivalent circuit based on the simple lumped model for a muscle fiber showing how the frequency-dependent transport number equivalent capacitance, C_{TN}, and resistance, R_{TN}, combine with the normal membrane capacitance C_m, and membrane resistance, R_m. R_i represents the internal resistance of the fiber which would become relevant in the cable clamp situation. Parameters are referred to unit area of fiber. At frequencies greater than 10 Hz, or in the absence of transport number effects, C_{TN} and R_{TN} both reduce to zero

In order to ensure minimal distortion of the sinusoidal nature of the voltage response because of the presence of anomalous rectification in muscle (e.g., Adrian & Freygang, 1962), it was necessary to use only a very small amplitude (e.g., 0.01 $\mu A \cdot cm^{-2}$) sinusoidal component of current. By itself this small amplitude current when injected into the muscle fiber illustrated that transport number effects were equivalent to a capacitance (C_{TN}) which increased from less than 1 $\mu F \cdot cm^{-2}$ at 10 Hz to about 16 $\mu F \cdot cm^{-2}$ at 0.01 Hz (as in Fig. 6) and to an equivalent dynamic membrane resistance which increased from its instantaneous slope value of 11.7 $k\Omega cm^2$ at 10 Hz to about 16 $k\Omega cm^2$ at very low frequencies (as in Fig. 5, with R_{TN} correspondingly increasing therefore from zero to about 4.3 $k\Omega cm^2$).

Furthermore in order to investigate equivalent capacitance effects during reasonably large, rectangular, hyperpolarizing and depolarizing

pulses, the small amplitude sinusoidal component was superimposed on rectangular pulses after the initial transient response to the pre-pulse had settled down (e.g., *see* Fig. 7). In the case of both $2.25\,\mu A \cdot cm^{-2}$ pulses, transport number effects gave rise to an equivalent capacitance (C_{TN}) which was less than $1\,\mu F \cdot cm^{-2}$ at 10 Hz, but then rose to a large maximum steady value of about $28\,\mu F \cdot cm^{-2}$ for the hyperpolarizing pulse and $24\,\mu F \cdot cm^{-2}$ for the depolarizing pulse at 0.01 Hz (as in Fig. 10). The equivalent dynamic resistances also increased from their instantaneous slope values of $4.7\,k\Omega cm^{-2}$ at 10 Hz to about $7.1\,k\Omega cm^2$ and $6.3\,k\Omega cm^2$ (with R_{TN} correspondingly increasing therefore from zero to about $2.4\,k\Omega cm^2$ and $1.6\,k\Omega cm^2$) for the hyperpolarizing and depolarizing pulses respectively at 0.01 Hz.

The effect of a large amplitude sinusoidal current ($2.25\,\mu A \cdot cm^{-2}$) by itself was also investigated. However, apart from the observation that transport number effects were causing large negative phase lags (Fig. 11) of the voltage response with respect to the current which implied that the effects were of a "capacitative" nature, particularly at very low frequencies, the distortion of the voltage waveform – resulting from the rectification characteristics – made any sort of an estimate of equivalent capacitance from a straightforward analysis of such phase lags quite invalid.

One of the more general predictions of this paper is the presence of a negative phase lag which in all cases considered was greater than 2° between 0.04 to 1.2 Hz and rose to a maximum value of 11.6° at about 0.35 Hz in the case of the small sinusoidal component superimposed on a $2.25\,\mu A \cdot cm^{-2}$ rectangular hyperpolarizing current pulse. For example, at a frequency of 1 Hz, the lower limit of many impedance analysis studies, the values of phase lags varied between $-2.2°$ and $-7.5°$ for the three cases studied by use of the small sinusoidal current component, and between $-2.9°$ and $-8.0°$ for the case of the large amplitude sinusoidal current by itself (e.g., Fig. 11). In order to compare such predictions with experimental studies it should, of course, be pointed out that this analysis corresponds to a space clamp situation with the current density constant along the length of the fiber (as is approximated at the end of the fiber in the 3-electrode clamp arrangement, e.g., Adrian, Chandler & Hodgkin, 1970*a*) and gives larger phase angles than the corresponding cable clamp with a point source injection of current. In fact, for a conventional RC circuit under space clamp conditions, the phase angle ϕ_s is given by:

$$\phi_s = \tan^{-1} \omega \tau$$

where ω is the frequency of the current in radian $\times \sec^{-1}$ and τ the time constant is given by:

$$\tau = R_m C_m.$$

On the other hand, for a cable clamp the phase angle ϕ_c is given (e.g., Tasaki & Hagiwara, 1957) by:

$$\phi_c = \tan^{-1}\left[\{(1+(\omega\tau)^2)^{\frac{1}{2}} - 1\}/\{(1+(\omega\tau)^2)^{\frac{1}{2}} + 1\}\right]^{\frac{1}{2}}$$
$$\simeq \tan^{-1}\left[\frac{\omega\tau}{2}(1-(\omega\tau/2)^2)\right] \quad \text{as} \quad \omega\tau \ll 1$$

and so $\phi_c \simeq \phi_s/2$ provided $\omega\tau \ll 1$ (e.g., if $\phi_s = 16°$, $\omega\tau = 0.287$, $\phi_c \simeq 7.99°$).

If the same sort of relationship is assumed between space and cable clamps for the component of phase angle resulting from transport number effects then, for example, even at 1 Hz one would predict an average negative phase angle of about 5° in the space clamp situation and about 2.5° in the cable clamp situation. This effect is maximum in a sulphate Ringer's solution and would be smaller in a chloride Ringer's solution. Nevertheless such negative phase angles seem to correspond reasonably well with the 2° deviation of experimental from expected values (the theoretical expected values being calculated from a number of equivalent circuits) obtained by Valdiosera, Clausen and Eisenberg (1974*b*, e.g., Fig. 2 of their paper) and would help to explain the discrepancy in their measurements on normal fibers at such low frequencies. It should also be emphasized, in support of this explanation for such a low frequency deviation, that Valdiosera *et al.* also found that the deviation decreased markedly in glycerol treated fibers (i.e., fibers with most of the transverse tubular system nonfunctional) and in otherwise normal fibers in which the resistance in series with the tubular system was strikingly high.

Probably the most important implication of the paper is, therefore, that a consideration of such transport number effects as outlined in this paper is critical for interpretation of any impedance studies carried out on skeletal muscle at very low frequencies, particularly at frequencies less than 1 Hz.

I would especially like to thank Dr. R. H. Adrian, with whom the original experimental work for *Paper 1* was done, the experimental parameters of which were used for the analysis in this paper.

I would also like to thank Mr. J. R. Smith for helpful discussions and Professor P. W. Gage, Dr. D. Van Helden, and Mr. J. R. Smith for their critical reading of the manuscript and resultant helpful comments. The assistance of Misses R. Diprose and F. Browne and Mrs. C. Prescott in preparation of the manuscript was also very much appreciated.

In addition, I would like to thank the Queen Elizabeth Fellowship Committee for a post-doctoral fellowship during the early stages of the project. The work was also supported by Australian Research Grants Committee – Grant D72/15201.

References

Adrian, R. H., Chandler, W. K., Hodgkin, A. L. 1969. The kinetics of mechanical activation in frog muscle. *J. Physiol.* (*London*) **204**:207

Adrian, R. H., Chandler, W. K., Hodgkin, A. L. 1970*a*. Voltage clamp experiments in striated muscle fibres. *J. Physiol.* (*London*) **208**:607

Adrian, R. H., Chandler, W. K., Hodgkin, A. L. 1970*b*. Slow changes in potassium permeability in skeletal muscle. *J. Physiol.* (*London*) **208**:645

Adrian, R. H., Freygang, W. H. 1962. The potassium and chloride conductance of frog muscle membrane. *J. Physiol.* (*London*) **163**:61

Almers, W. 1972*a*. Potassium conductance changes in skeletal muscle and the potassium concentration in the transverse tubules. *J. Physiol.* (*London*) **225**:33

Almers, W. 1972*b*. The decline of potassium permeability during extreme hyperpolarisation in frog skeletal muscle. *J. Physiol.* (*London*) **225**:57

Barry, P. H. 1976. Transport number effects in the transverse tubular system of muscle and their effects on low frequency A/C impedance analysis. *Proc. Aust. Physiol. Pharmacol. Soc.* **7**:4*P*

Barry, P. H., Adrian, R. H. 1973. Slow conductance changes due to potassium depletion in the transverse tubules of frog muscle fibers during hyperpolarizing pulses. *J. Membrane Biol.* **14**:243

Barry, P. H., Hope, A. B. 1969*a*. Electroosmosis in membranes: Effects of unstirred layers and transport numbers. I. Theory. *Biophys. J.* **9**:700

Barry, P. H., Hope, A. B. 1969*b*. Electroosmosis in membranes: Effects of unstirred layers and transport numbers. II. Experimental. *Biophys. J.* **9**:729

Coster, H. G. L., Smith, J. R. 1974*a*. The effect of pH on the low frequency capacitance of the membranes of *Chara corallina*. *In:* Membrane Transport in Plants. Pp. 154–161. U. Zimmermann and J. Dainty, editors. Springer-Verlag, Heidelberg

Coster, H. G. L., Smith, J. R. 1974*b*. The molecular organisation of bimolecular lipid membranes. A study of the low frequency Maxwell-Wagner impedance dispersion. *Biochim. Biophys. Acta* **373**:151

Dewhurst, D. J. 1960. Concentration polarisation in plane membrane-solution systems. *Trans. Faraday Soc.* **56**:599

Eisenberg, R. S., Gage, P. W. 1969. Ionic conductances of the surface and transverse tubular membranes of frog sartorius fibers. *J. Gen. Physiol.* **53**:279

Endo, M. 1966. The entry of fluorescent dyes into the sarcotubular system of the frog muscle. *J. Physiol.* (*London*) **185**:224

Huxley, H. F. 1964. Evidence for continuity between the central elements of the triads and the extracellular space in frog sartorius muscle. *Nature* (*London*) **202**:1067

Katz, B. 1949. Les constantes électriques de la membrane du muscle. *Arch. Sci. Physiol.* **3**:285

McCracken, D. D. 1965. A Guide to Fortran IV Programming. John Wiley and Sons, New York

Mobley, B. A., Eisenberg, B. R. 1975. Sizes of components in frog skeletal muscle measured by methods of sterology. *J. Gen. Physiol.* **66**:31

Page, S. G. 1964. The organisation of the sarcoplasmic reticulum in frog muscle. *J. Physiol.* (*London*) **175**:10*P*

Peachey, L. D. 1965. The sarcoplasmic reticulum and the transverse tubules of the frog's sartorius. *J. Cell. Biol.* **25**:209

Ralston, A. 1965. A First Course in Numerical Analysis. McGraw-Hill, New York

Schaefer, H., Scholmerich, P., Haass, P. 1939. Der Elektrotonus und die Erregungsgesetze des Muskels. *Pfluegers Arch. Gesamte Physiol.* **241**:310

Segal, J.R. 1967. Electrical capacitance of ion-exchanger membranes. *J. Theor. Biol.* **14**:11

Sokolnikoff, I. S., Redheffer, R. M. 1958. Mathematics of Physics and Modern Engineering. McGraw-Hill, New York

Tasaki, I., Hagiwara, S. 1957. Capacity of muscle fiber membrane. *Am. J. Physiol.* **188**:423

Valdiosera, R., Clausen, C., Eisenberg, R. S. 1974*a*. Circuit models of the passive electrical properties of frog skeletal muscle fibers. *J. Gen. Physiol.* **63**:432

Valdiosera, R., Clausen, C., Eisenberg, R. S. 1974*b*. Impedance of frog skeletal muscle fibers in various solutions. *J. Gen. Physiol.* **63**:460

Wedner, H. J., Diamond, J. M. 1969. Contributions of unstirred-layer effects to apparent electrokinetic phenomena in the gall bladder. *J. Membrane Biol.* **1**:92